Artificial Organs

A Dermal Equivalent Engineered with TGF-β3 Expressing Bone Marrow Stromal Cells and Amniotic Membrane: Cosmetic Healing of Full-Thickness Skin Wounds in Rats

*†‡Ali Samadikuchaksaraei, †Ahmad Mehdipour, §Mehryar Habibi Roudkenar, **Javad Verdi, *Mohammad Taghi Joghataei, ††Kamran As'adi, §Fatemeh Amiri, ‡‡Mozhgan Dehghan Harati, *†§§Mazaher Gholipourmalekabadi, and ***Nushin Karkuki Osguei

*Cellular and Molecular Research Center, Iran University of Medical Sciences; †Department of Tissue Engineering & Regenerative Medicine, Faculty of Advanced Technologies in Medicine, Iran University of Medical Sciences; ‡Department of Medical Biotechnology, Faculty of Allied Medicine, Iran University of Medical Sciences, Tehran; §Department of Medical Biotechnology, Faculty of Allied Medicine, Guilan University of Medical Sciences, Rasht; **Department of Applied Cellular Sciences, Faculty of Advanced Technologies in Medicine, Tehran University of Medical Sciences; ††Department of Plastic and Reconstructive Surgery, Faculty of Medicine, Iran University of Medical Sciences, Tehran, Iran; ‡‡Translational Oncology, Department of Hematology, Oncology, Immunology, Rheumatology and Pulmonology, University Hospital Tuebingen, Tuebingen, Germany; §§Department of Medical Biotechnology, Faculty of Medicine, Shahid Beheshti University of Medical Sciences; and ***Eposcience Millennium Institute, Tehran, Iran

Abstract: Transforming growth factor beta-3 (TGF-β3) has been shown to decrease scar formation after scheduled topical applications to the cutaneous wounds. This study aimed to continuously deliver TGF-β3, during the early phase of wound healing, by engineering a dermal equivalent (DE) using TGF-β3 expressing bone marrow stromal cells (BM-SCs) and human dehydrated amniotic membrane (hDAM). To engineer a DE, rat BM-SCs were seeded on the hDAM and TGF-β3 was transiently transfected into the BM-SCs using a plasmid vector. Pieces of the dermal equivalent were transplanted onto the full-thickness excisional skin wounds in rats. The process of wound healing was assessed by image analysis, Manchester Scar Scale (MSS), and histopathological studies 7, 14, 21, and 85 days after the excision. The results confirmed accurate construction of recombinant pcDNA3.1-TGF-β3 expression system and showed that the transfected BM-SCs seeded on hDAM expressed TGF-β3 mRNA and protein from day 3 through day 7 after transfection. After implantation of the DE, contraction of the wounds was measured from day 7 through 21 and analyzed by linear regression, which revealed that the rate of wound contraction in all experimental groups was similar. Histologic evaluation demonstrated that transfected BM-SCs decreased retention and recruitment of the cells during the early stage of wound healing, decreased the formation of vascular structures and led to formation of uniformly parallel collagen bundles. MSS scores showed that TGF-β3 secreting cells significantly improved the cosmetic appearance of the healed skin and decreased the scar formation. From these results, it could be concluded that transient secretion of TGF-β3, during the early phase of healing, by BM-SCs seeded on hDAM can improve the cosmetic appearance of the scar in cutaneous wounds without negatively affecting the process of wound repair. **Key Words:** Cicatrix—Keloid—Re-epithelialization—Scar—Transforming growth factor beta-3.

Scar tissue formation following the process of cutaneous wound healing can lead to cosmetically less acceptable appearance depending on the site and extent of the wound. Several strategies have been adopted to reduce the formation of scar tissue during wound healing including manipulation of the active biochemical factors participating in this

doi: 10.1111/aor.12807

Received April 2016; revised June 2016.

The first two authors contributed equally to this work.
Ali Samadikuchaksaraei senior author.

Address correspondence and reprint requests to Dr. Ali Samadikuchaksaraei, Department of Tissue Engineering and Regenerative Medicine, Iran University of Medical Sciences, Hemmat Highway, Tehran 144961-4535, Iran. E-mail: samadikuchaksaraei@yahoo.com

process. In recent years, transforming growth factor beta (TGF-β) signaling pathway has attracted much attention as a suitable target for manipulation of the process of cutaneous repair (1). The pattern of expression and the temporal appearance of three isoforms of TGF-β including TGF-β1, TGF-β2, and TGF-β3, play an important role in regulation of the mechanisms that lead to wound healing (2).

TGF-β1 and TGF-β2 act as homing factors for inflammatory cells and fibroblasts, promote synthesis and deposition of main extracellular matrix (ECM) components, inhibit matrix metalloproteinases (MMPs) to enhance accumulation of ECM, induce fibroblast differentiation and angiogenesis, and regulate keratinocytes migration (3). TGF-β3 balances the actions of TGF-β1 and TFF-β2 by decreasing the fibroblast migration and differentiation, reducing the ECM synthesis, promoting the activity of the MMPs (see Pakyari et al., 2013 for review [4]), and decreasing the density of wound epithelialization (5). In summary, scar tissue formation is increased by TGF-β1 and TGF-β2 and decreased by TGF-β3. The latter is expressed at high levels in developing skin and is the main factor responsible for scarless wound healing during the fetal period (6). Also, in oral mucosal wounds, in which healing is characterized by minimal scar formation, the proportion of TGF-β3/TGF-β1 is much higher than cutaneous wounds (7). In other words, the high proportion of TGF-β1 and TGF-β2 to TGF-β3 in adult skin wounds is the key regulatory mechanism that favors scar formation (8,9). It should be noted that in skin wounds, keeping the above proportion, the level of TGF-β3 during the early phase of healing is higher than other phases (10).

Local administration of TGF-β3 to decrease scarring and improve the cosmetic appearance of the healing wound has been studied in several animal models with promising results (11–14). This led to translation of these studies into the phase I/II clinical trials by Renovo (Manchester, UK) (15). In these clinical trials, the recombinant, active human TGF-β3 (Avotermin) was intradermally administered in healthy subjects to the margins of full-thickness incisions before and after the operation. The product has been shown to be effective for cosmetic healing of the wounds. However, in the phase III clinical trial, Avotermin failed to meet its efficacy endpoints and further evaluation of this product has been discontinued (16).

In the above studies, TGF-β3 protein was locally delivered to the site of injury at scheduled time intervals. We hypothesized that this method does not secure a continuous delivery of TGF-β3 in the wound area over the prescribed period. As temporal variation in TGF-β3 levels in the healing tissue is a critical determinant of the degree of scarring, we aimed in this study to continuously deliver TGF-β3 by genetically engineered bone marrow stromal cells, which transiently express this protein. In addition, these genetically modified cells were used to engineer a dermal equivalent using human dehydrated amniotic membrane (hDAM) (patent pending).

It has been known for a long time that synthetic (17), semisynthetic (18–20), and natural scaffolds (21) can enhance the regenerative process in the injured tissues. Of natural scaffolds, amniotic membrane has been successfully used to promote skin wound healing. It has been shown that hDAM contains detectable levels of several different cytokines which affect wound healing (see Koob et al., 2015 for the list [22]). The main cytokines reported in hDAM include: (1) cytokines that promote homing of stem cells such as stromal cell-derived factor 1 (SDF-1) (23); (2) cytokines that increase proliferation and migration of keratinocytes such as epidermal growth factor, basic fibroblast growth factor, TGF-α, and hepatocyte growth factor (23); (3) cytokines that attenuate inflammatory response such as interleukins 4, 6, 8, and 10 (22); (4) cytokines that increase deposition of extracellular matrix such as TGF-β1 (4); (5) cytokines that inhibit matrix metalloproteinases such as tissue inhibitors of metalloproteinases 1, 2, and 4 (24). The effects of extracellular matrix of hDAM, including basement membrane (25), on wound healing is of importance as well. The main ECM components of amniotic membrane are laminin, fibronectin, types I, III, IV, V, VI, and VII collagens, decorin, biglycan, hyaluronic acid, and elastin (26). These components regulate the wound healing process including cell proliferation, migration, angiogenesis, and deposition of ECM. Their effects on reduction of scar formation has also been reported (27). These properties of the amniotic membrane make it an excellent scaffold for engineering of a dermal equivalent. Here, we aim to engineer a dermal equivalent with TGF-β3 expressing bone marrow stromal cells and amniotic membrane to modulate cosmetic healing of full-thickness skin wounds.

MATERIALS AND METHODS

Isolation and culture of bone marrow-derived stromal cells

Bone marrow-derived stromal cells (BM-SCs) were isolated from femur and tibia of male Wistar rats, weighing 200 g. The animals were maintained in

TABLE 1. *Transforming growth factor β3 (TGF-β3) and beta actin primers*

Marker	Forward primer	Reverse primer	Amplicon size
TGF-β3	TAGCTAGCATGGTGAAGATGCACTTGCAAAG	CACTCGAGTCAGCTACATTTACAAGACTTC	1239 bp
Beta actin	TTCTACAATGAGCTGCGTGTGG	GTGTTGAAGGTCTCAAACATGAT	115 bp

accordance with the local Animal Care Committee guidelines in the Animal House of Iran University of Medical Sciences. Briefly, the rats were sacrificed by CO_2 asphyxiation and the tibia and femur bones were harvested. Then, both ends of the bones were aseptically cut off by scissors, and bone marrow was flushed into 25 cm^2 cell culture flasks by Low-Glucose Dulbecco's Modified Eagle's Medium (DMEM-LG; Gibco, Eggenstein, Germany) supplemented with 10% (v/v) fetal bovine serum (FBS; Sigma, St. Louis, MO, USA), penicillin (100 U/mL), and streptomycin (100 μg/mL) (Biosera, Sussex, UK). The flasks were then taken into a humidified incubator (37°C, 5% CO_2) and passaged at 80% confluency using trypsin-EDTA 0.25% (Biosera). The cells were transfected at passage 4.

Construction of recombinant pcDNA3.1-TGF-β3 expression system

PCR amplification of rat TGF-β3 cDNA sequence was performed from the cloning vector pGEM-T-TGF-β3 (Sino Biological Company, Beijing, China) using the primers presented in Table 1. The PCR amplification was performed in GeneAmp PCR system 9600 (PerkinElmer Life and Analytical Sciences, Wellesley, MA, USA) with 25 cycles of denaturation (at 95°C for 30 s), annealing (at 60°C for 30 s), and elongation (at 72°C for 1 min). Then, pcDNA3.1 plasmid vector (Invitrogen, Carlsbad, CA, USA) and the PCR product were digested with NheI and XhoI (Fermentas, Burlington, ON, Canada) restriction enzymes. To construct the recombinant vector pcDNA3.1-TGF-β3, the TGF-β3 full-length cDNA was ligated to pcDNA3.1 using the T4 DNA ligase enzyme (Roche, Mannheim, Germany). The accuracy of ligation was confirmed by PCR using the primers presented in Table 1. Following successful ligation, the pcDNA3.1-TGF-β3 was transformed into the competent *Escherichia coli* bacteria (Sinnagen, Tehran, Iran) using heat (42°C) and cold (0°C) shocks. The success of transformation was confirmed by extraction of plasmids from the transformed bacteria by plasmid extraction kit (Roche), and PCR confirmation with the same primers presented in Table 1. Finally, using the primer pair presented in Table 2, the cloned pcDNA3.1-TGF-β3 vector was sequenced (Microgen, Seoul, South Korea) to verify the accuracy of the reading frame of TGF-β3 inside the vector.

Cell seeding on human dehydrated amniotic membrane

A commercially available human dehydrated amniotic membrane (hDAM) (AmnioFix, MiMedx Group, Inc., Marietta, GA, USA) was aseptically cut into 2 × 2 cm pieces and placed in 6-well plates (Orange Scientific, Brussels, Belgium). One day before cell seeding, pieces of the membrane were soaked with culture medium and kept in a humidified incubator (37°C, 5% CO_2). Then, 4×10^5 BM-SCs in 100 μL of culture medium were loaded on each piece of the membrane, and the pieces were put in the incubator for 2 h. Finally, the wells were filled with 2 mL of DMEM, supplemented with 10% FBS (v/v), penicillin (100 U/mL), and streptomycin (100 μg/mL), and maintained in the incubator for 48 h.

Transfection of BM-SCs with pcDNA3.1-TGF-β3

The day before transfection, BM-SCs-seeded membranes were incubated in DMEM (without antibiotics). The transfection process was performed by incubating the cells in the DNA transfection complex containing 500 μL of DMEM without antibiotics, 2 μg pcDNA3.1-TGF-β3, and 9 μL Lipofectamin 2000 transfection reagent (Invitrogen, Karlsruhe, Germany). Following 4 h of incubation at 37°C in a humidified 5% CO_2 incubator, transfection complex was replaced with DMEM, supplemented with 10% FBS (v/v), 100 U/mL penicillin, and 100 μg/mL streptomycin. From the first day after transfection (day 1) through day 9, the cells were harvested daily for RT-PCR and Western blotting to confirm expression of TGF-β3 at mRNA and protein levels.

RT-PCR

The BM-SCs transfected with pcDNA3.1 empty vector and those transfected with pcDNA3.1-TGF-β3 were subjected to RNA extraction using Trizol (Roche). Total cDNA was generated from 1 μg of the extracted total RNA using cDNA synthesis kit (Invitrogen, Carlsbad, CA, USA). To determine the TGF-β3 mRNA levels, RT-PCR was carried out using the primers in Table 1. Beta-actin was used as an internal control.

TABLE 2. *The cloned pcDNA3.1-TGF-β3 vector primers*

Primer name	Primer sequence	Amplicon size
T7 promoter, forward primer	TAATACGACTCACTATAGGG	1239 bp
BGH, reverse primer	TAGAAGGCACAGTCGAGG	

BGH, bovine growth hormone terminator.

Western blotting

The secretome of the cells transfected with pcDNA3.1-TGF-β3 and of those transfected with pcDNA3.1 empty vector was concentrated by Vivaspin concentrator (Sartorius Stedim Biotech, Goettingen, Germany), loaded on a 12% SDS-polyacrylamide gel, and transferred onto a PVDF membrane through semidry blotting. The membrane was subsequently incubated in rabbit anti-TGF-β3 polyclonal primary antibody (1:200, Signalway, Nanjing, China) at 4°C overnight. Then, the membrane was covered with goat anti-rabbit HRP-conjugated secondary antibody (1:5000, Signalway). Finally, ECL chemiluminescent substrate (Abcam, Cambridge, UK) was added to the membrane, and the expected protein bands were visualized by the ChemiDoc MP imaging system (Biorad, Hercules, CA, USA). Rabbit anti-beta-actin polyclonal antibody (1:3000, Abcam) was used for detection of beta-actin, as an internal control.

In vivo studies

Forty-eight 10-week-old male Wistar rats (200 − 220 g) were maintained in individual cages in accordance with the local Animal Care Committee guidelines in the Animal House of Iran University of Medical Sciences. The animals were acclimatized for one week before the experiment under environmentally controlled conditions (22–23°C temperature on a 12:12 h light:dark cycle).

Full-thickness excisional skin wound model

At the time of the experiment, the rats were anesthetized by intraperitoneal injection of a ketamine:xylazine (70:7 mg/kg) cocktail. Under deep anesthesia, the upper back region of all rats was shaved and prepped with 10% povidone iodine. Then, the skin was marked 5 cm below the skull base by a square of 2 × 2 cm and the epidermis, dermis, and panniculus carnosus muscle were totally removed using a sterile scalpel. As human lacks the panniculus carnosus at the base of the dermis and this muscle leads to the contraction of the wound bed in rats, it has been removed to properly simulate the human full-thickness skin wound.

All animals were randomly assigned into four groups ($n = 3$) of (1) control (C), in which the defect area was only washed with phosphate-buffered saline (PBS); (2) amniotic membrane (A), in which the defect area was implanted with human dehydrated amniotic membrane (hDAM) alone; (3) amniotic membrane seeded with untransfected BM-SCs (AUB), in which the defect area was implanted with hDAM seeded with untransfected rat BM-SCs; and (4) amniotic membrane seeded with transfected BM-SCs (ATB), in which the defect was implanted with the hDAM seeded with TGF-β3-expressing rat BM-SCs. To avoid the possible postoperative infection, all animals were given an oral daily dose of cephalexin (5 mg/10 mL water) from the day of operation through the fifth postoperative day.

Implantation

The implants were used 3 days after transfection of BM-SCs. Immediately after full-thickness skin removal, the implant was immersed in sterile PBS solution, grafted to the wound area and covered by a transparent wound dressing (Comfeel Plus, Coloplast, Humlebæk, Denmark) (28). Finally, the rats were maintained in individual cages and received daily check-ups until tissue sampling.

Skin evaluation and tissue sampling

The defect areas were examined by taking photographs at different time points (day of surgery [0] and days 7, 14, 21, and 85). In each photograph, the area of the defect was measured by the measurement tool of Adobe Photoshop CS6 (v.13.0.1 Extended) software (Adobe System, Inc., Seattle, WA, USA). Before taking photographs, a ruler was placed across the defects to confirm the accuracy of measurements. The percentage of wound contraction was calculated using the formula suggested by Shenoy et al., 2011 (29):

$$\text{Wound Contraction } (\%) = \left[\frac{\text{Initial Wound Size} - \text{Specific Day Wound Size}}{\text{Initial Wound Size}}\right] \times 100$$

The scar tissue was assessed using the Manchester Scar Scale (MSS) proposed by Beausang et al., 1998 (30) and reviewed by Fearmonti et al., 2010 (31). MSS evaluates the following parameters

including: color (perfect [score 1]; mismatch to surrounding tissue: slight [score 2], obvious [score 3], gross [score 4]), glossiness (matte [score 1], shiny [score 2]), levelness with surrounding (flush [score 1], slightly proud/indented [score 2], hypertrophic [score 3], keloid [score 4]), distortion (none [score 1], mild [score 2], moderate [score 3], severe [score 4]), and texture (normal [score 1], just palpable [score 2], firm [score 3], hard [score 4]).

As we aimed to decrease the scar tissue and the effects of interventions that affect the formation of scar tissue in rat skin will be detectable only after the 80th postoperative day (32), the animals were evaluated on day 85 for Manchester Scar Scale. The scores of individual parameters were added to obtain the overall MSS score, which ranged from 5 (perfect) to 18 (poor). The assessments were performed by three independent observers in blinded fashion.

Full-thickness skin samples were taken from wound areas on days 7, 14, 21, and 85 following surgery. Tissue specimens were then fixed in 10% formaldehyde, dehydrated in graded alcohol solutions of 50, 70, 90, 96, and 100%, cleared in xylene (Merck, Darmstadt, Germany), and embedded in paraffin (Merck). Next, tissue specimens were cut into 5-μm thick slices, mounted onto glass slides, and underwent hematoxylin and eosin (H&E) staining. The number of cells and vessels in the healing tissue were counted using 40× magnification on days 7, 14, and 21. In each slide, three fields (middle, top, and bottom) were counted and averaged. The cells were counted by enumeration of the cell nuclei. The vessels were identified by lumen-like structures filled by erythrocytes (33). Masson's trichrome staining was also performed to visualize the formation and orientation of collagen fibers on days 21 and 85.

Statistical analysis

Linear regression has been used for analysis of wound contraction. The contraction values were plotted against the days of measurement and a line was fitted to the data in each experimental group. The best fit lines were compared by linear regression analysis using GraphPad Prism (Prism 5, v5.03, 2009, GraphPad Prism Software Inc., San Diego, CA, USA). The goodness of fit of each line was accepted when R^2 was higher than 0.80. The slopes and elevations of the trendlines were considered to be significantly different when the P value was less than 0.05. For comparison of means, the normality of distribution of the data was assessed by the Shapiro–Wilk test. For data with normal distribution, the Levene Statistic was used to confirm homogeneity of variances. The means with equal variances were compared by one-way ANOVA followed by Tukey's post hoc test. The means with unequal variances were compared by one-way ANOVA weighted by Dunnett's T3 post hoc test. For the data deviated from normal distribution, Kruskal–Wallis one-way ANOVA with "all pair-wise" comparisons was used for comparison of means. The data were analyzed by IBM SPSS Statistics (v21, IBM Corp., Armonk, NY, USA). The means were considered to be significantly different when the P value was less than 0.05.

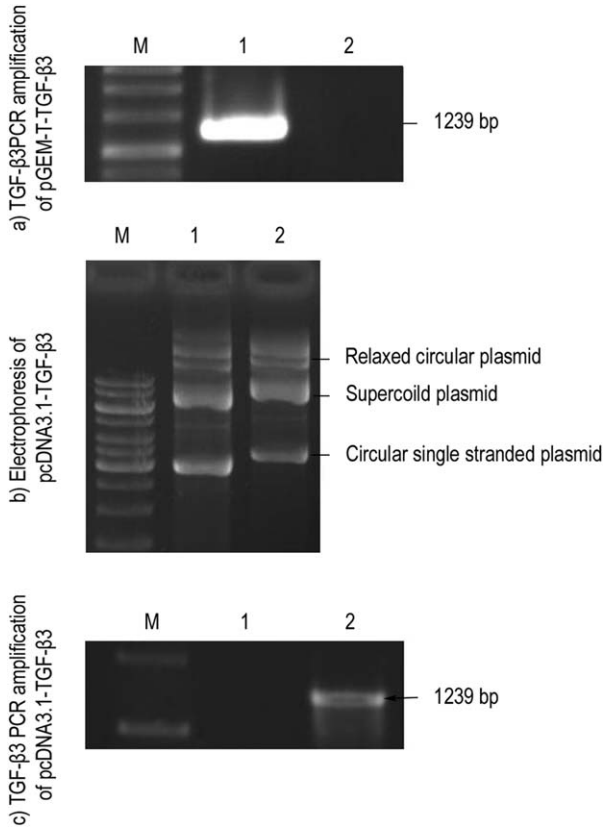

FIG. 1. Subcloning of TGF-β3 into pcDNA3.1 vector. (a) PCR amplification of the full-length TGF-β3 cDNA; TGF-β3 was successfully isolated from pGEM-T-TGF-β3 vector (lane 1). (b) Electrophoresis of pcDNA3.1-TGF-β3; lane 1: empty pcDNA3.1 vector, lane 2: pcDNA3.1-TGF-β3. pcDNA3.1-TGF-β3 moved slower than empty pcDNA3.1 on agarose gel. M: 1000 bp DNA marker. (c) PCR amplification of TGF-β3 sequence of pcDNA3.1-TGF-β3 plasmid vector isolated from the transformed *E. coli* bacteria; lane 1: empty pcDNA3.1, lane 2: pcDNA3.1-TGF-β3. The 1239 bp PCR product confirmed the insertion of TGF-β3 into the pcDNA3.1 vector.

RESULTS

Isolation and culture of bone marrow–derived stromal cells

The isolated bone marrow cells that formed adherent cultures and showed a spindle-shaped morphology

were cultured and passaged for four times. At passage 4, the cells were harvested and seeded on the dehydrated amniotic membrane.

Construction of recombinant pcDNA3.1-TGF-β3 expression system

In this stage, the TGF-β3 gene was sub-cloned into the pcDNA3.1 vector. Figure 1a shows the PCR product amplified from pGEM-T-TGF-β3 vector. The amplicon size of 1239 bp conforms to the size of TGF-β3 cDNA. After restriction enzyme digestion and ligation of TGF-β3 cDNA to pcDNA3.1, the accuracy of ligation was confirmed by electrophoresis of pcDNA3.1-TGF-β3 and pcDNA3.1 empty vector in 1% agarose gel (Fig. 1b). The slower movements of relaxed circular, supercoiled, and circular single-stranded pcDNA3.1-TGF-β3 compared with the empty plasmid indicated insertion of the TGF-β3 cDNA into the pcDNA3.1 vector.

PCR amplification of TGF-β3 sequence of pcDNA3.1-TGF-β3 plasmid vector isolated from the transformed *E. coli* bacteria (Fig. 1c) detected an amplicon size of 1239 bp, which conformed to the size of TGF-β3 cDNA. The result of sequencing of the cloned pcDNA3.1-TGF-β3 vector confirmed that TGF-β3 cDNA was accurately inserted in the vector.

Cell seeding on the hDAM and transfection

As shown in Fig. 2, seeding of the rat BM-SCs on the human dehydrated amniotic membrane (hDAM) was successfully carried out and the cells were evenly distributed on the hDAM. After transfection of BM-SCs with pcDNA3.1-TGF-β3, the RT-PCR and Western blotting were carried out to confirm TGF-β3 mRNA and protein expression by the transfected cells. The cells were harvested for analysis until day 9 after transfection. The results showed that the transfected cells express TGF-β3 mRNA and protein from day 3 through day 7 after transfection. The cells transfected with pcDNA3.1 empty vector showed no band formation at the expected band size. Figure 3 shows a representative gel of the RT-PCR and the representative Western blot bands of these studies.

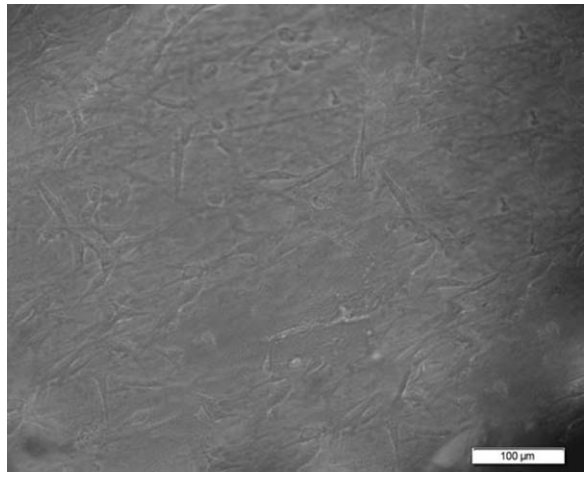

FIG. 2. Cell seeding on dehydrated amniotic membrane. Phase-contrast inverted micrograph showing attachment of rat bone marrow stromal cells on human dehydrated amniotic membrane after 24 h of culture; scale bar 100 μm.

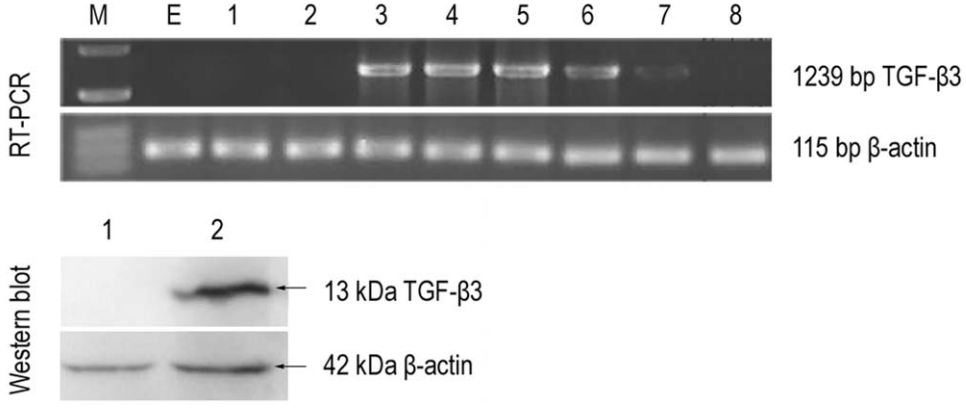

FIG. 3. RT-PCR and Western blot analysis of transfected cells. The TGF-β3 mRNA and protein were detected by RT-PCR and Western blot analyses of rat bone marrow stromal cells transfected with pcDNA3.1-TGF-β3 vector. The representative RT-PCR bands show expression of TGF-β3 mRNA from day 3 through 7 after transfection (M molecular marker, E control cells transfected with empty vector, lanes 1 through 8 represent the corresponding days after transfection). The Western blot bands show the representative bands on day 3 after transfection (lane 1 control cells transfected with empty vector, lane 2 day 3 transfected cells). Beta-actin was used as an internal control.

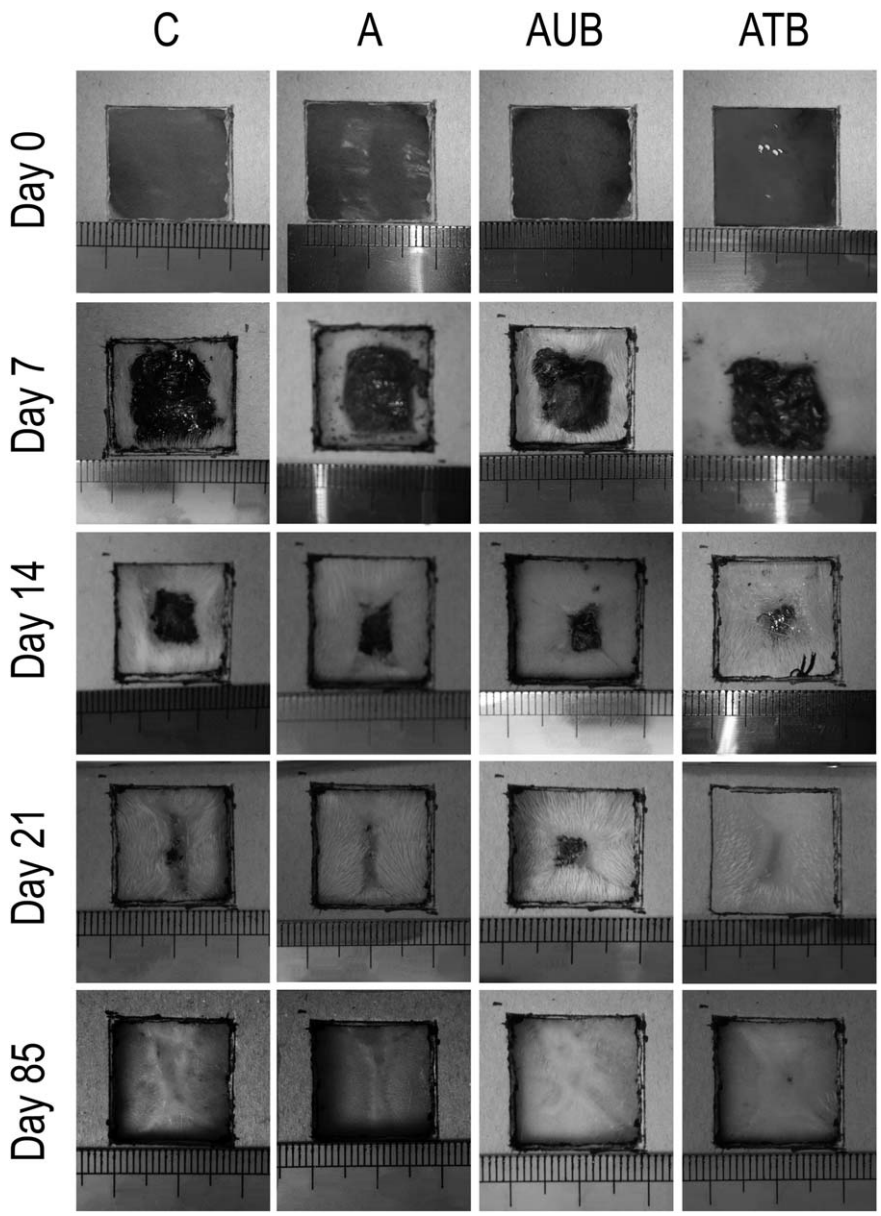

FIG. 4. Macroscopic photographs of the rat skin wounds. Photographs were taken to measure the wound surface areas in the experimental animal groups on the day of surgery (day 0) and postoperative days 7, 14, 21, and 85. Photographs on day 85 indicated a cosmetically more acceptable appearance of the healing wound in the ATB group compared to others. Dimensions of the wounds are measured by the ruler shown in each photograph. The smallest division of the ruler depicted in the photos is 1 mm. C, control group with no implantation; A, group implanted with human dehydrated amniotic membrane (hDAM) alone; AUB, group implanted with the hDAM seeded with untransfected bone marrow stromal cells (BM-SCs); ATB, group implanted with the hDAM seeded with the transfected BM-SCs.

In vivo studies

Macroscopic evaluation of wound closure

None of the rats entered into the study showed any sign of wound infection postoperatively. Figure 4 shows the representative photographs of the defect areas in the animal groups from the day of surgery (day 0) through day 85. The measurement of the wound contractions from day 7 through 21 was plotted in a scatter chart (Fig. 5) and a linear regression line was fitted to the dataset in each group. As presented in Table 3, linear regression analysis showed that the difference in slopes and elevations of the lines are not statistically significant ($P > 0.05$). This means that the rate of wound contraction in all four experimental groups was similar.

The Shapiro–Wilk test showed normality of distribution of MSS scores ($P > 0.05$) and the Levene Statistic confirmed equality of variances ($P > 0.05$). Therefore, one-way ANOVA followed by Tukey's post hoc test were used for statistical analysis. Figure 6 and Table 4 show the means and comparison of MSS scores in the experimental groups on day 85. MSS scores showed that TGF-β3 secreting cells significantly improved the cosmetic appearance of the healed skin and decreased the scar formation. On the other hand, no significant difference was

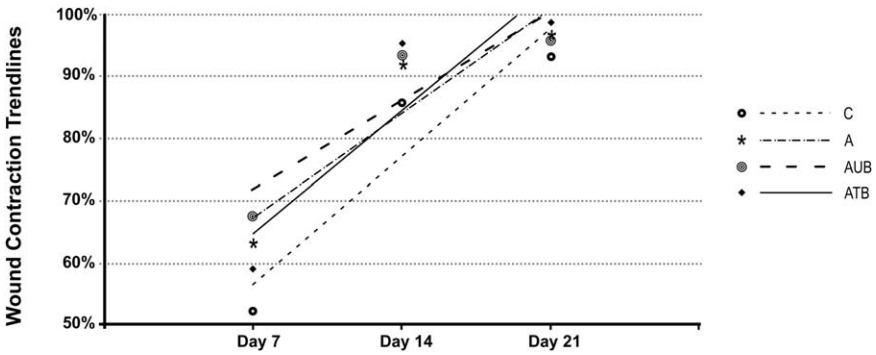

FIG. 5. Wound contraction in the experimental groups. The percentage of wound contraction has been plotted from day 7 through 21 as a scatter plot with linear regression lines fitted to each experimental group. C, control group with no implantation; A, group implanted with human dehydrated amniotic membrane (hDAM) alone; AUB, group implanted with the hDAM seeded with untransfected bone marrow stromal cells (BM-SCs); ATB, group implanted with the hDAM seeded with the transfected BM-SCs.

observed between the group treated with the hDAM and the group treated with hDAM seeded with untransfected BM-SCs ($P = 0.630$).

Histological results

Morphologic evaluation of the histological sections detected epithelialization of the wounds in all experimental groups from the first day of sampling on seventh postoperative day. The fragile epithelium identified on day 7 progressed to a more stable and multilayer epithelium in subsequent samplings from day 14th (Fig. 7). Wound epithelialization followed the same pattern in all experimental groups. Representative photomicrographs of the healing dermis in all experimental groups are presented in Fig. 8. From day 7 through 21, the cell numbers and vascularity decreased progressively in the healing tissues. The pattern was fairly uniform in all experimental groups.

Figure 9 represents the 40× magnification of the microscopic field used for counting of cell nuclei and vascular structures. For cell nuclei counting data, on day 7, one-way ANOVA weighted by the Welch method and followed by Dunnett's T3 post hoc were used for analysis of data. For days 14 and 21 nuclei counting data, one-way ANOVA followed by Tukey's post hoc test were used for statistical analysis. Figure 10 shows the result of nuclear counting and the significant differences. On day 7, the total number of cells in AUB group is higher than all others and in ATB group is lower than the other groups. On day 14, total cell numbers in AUB and ATB groups are lower than control and A groups. Also, the cell number in the A group is lower than the controls. Cell counting on day 21 does not show any statistically significant difference between the experimental groups.

TABLE 3. *Details of the linear regression lines fitted to the dataset in each experimental group*

Experimental group	R^2	Slope	*Y*-intercept
C	0.88	2.93 ± 1.07	36.13 ± 16.21
A	0.85	2.39 ± 0.98	50.53 ± 14.90
AUB	0.82	2.04 ± 0.94	57.37 ± 14.28
ATB	0.81	2.82 ± 1.36	45.03 ± 20.52
P value		0.93	0.63

C, control group with no implantation; A, group implanted with human dehydrated amniotic membrane (hDAM) alone; AUB, group implanted with the hDAM seeded with untransfected bone marrow stromal cells (BM-SCs); ATB, group implanted with the hDAM seeded with the transfected BM-SCs.

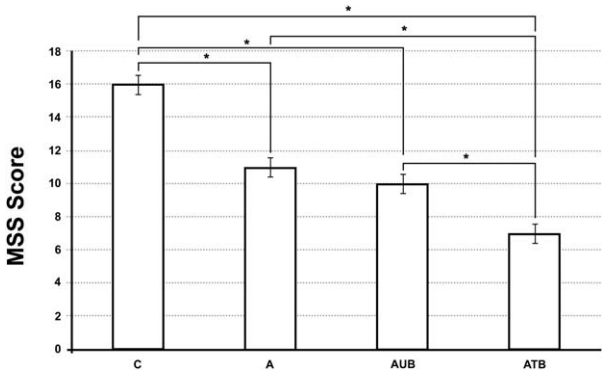

FIG. 6. The mean scores of Manchester Scar Scale. The appearance of the wounds in four experimental groups were compared 85 days postimplantation. Except the difference between A and AUB, the differences of other groups were statistically significant (indicated by asterisks, see Table 4). The best cosmetic appearance was achieved by application of ATB. MSS, Manchester Scar Scale; C, control group with no implantation; A, group implanted with human dehydrated amniotic membrane (hDAM) alone; AUB, group implanted with the hDAM seeded with untransfected bone marrow stromal cells (BM-SCs); ATB, group implanted with the hDAM seeded with the transfected BM-SCs.

TABLE 4. *Pair-wise comparison of MSS scores in experimental groups by Tukey's post hoc test*

Comparing groups	Mean difference	*P* value
Group C versus		
Group A	5.00	0.001
Group AUB	6.00	< 0.001
Group ATB	9.00	< 0.001
Group A versus		
Group C	−5.00	0.001
Group AUB	1.00	0.630
Group ATB	4.00	0.005
Group AUB versus		
Group C	−6.00	< 0.001
Group A	−1.00	0.630
Group ATB	3.00	0.026
Group ATB versus		
Group C	−9.00	< 0.001
Group A	−4.00	0.005
Group AUB	−3.00	0.026

MSS, Manchester Scar Scale; C, control group with no implantation; A, group implanted with human dehydrated amniotic membrane (hDAM) alone; AUB, group implanted with the hDAM seeded with untransfected bone marrow stromal cells (BM-SCs); ATB, group implanted with the hDAM seeded with the transfected BM-SCs.

For the counts of vascular structures on days 7 and 21, the statistical analysis was performed by one-way ANOVA followed by Tukey's post hoc test. For the day 14 vascular counts, Kruskal–Wallis one-way ANOVA with "all pair-wise" comparisons was employed. The results showed no statistically significant difference between the groups on day 7 ($P > 0.05$); a significantly lower number of vessels in AUB group compared to controls on day 14 ($P < 0.05$); and a significantly lower number of vessels in groups A, AUB, and ATB compared to controls on day 21 ($P < 0.05$) (Fig. 11).

Masson's trichrome staining of scar tissue on postoperative days 21 and 85 (Fig. 12) showed the formation and organization of the collagen bundles. As expected, the bundles were more organized on day 85 compared to day 21. On day 21, the organization of collagen bundles was similar in all groups. However, on day 85, the bundles showed higher organization in the rats that received an implant. In the control group with no implantation, the collagen bundles were extended in all directions. The wounds implanted with human dehydrated amniotic membrane (hDAM) only, or hDAM seeded with untransfected stromal cells, showed a higher organization of bundles as compared with the control group. The best histological result was obtained in the group implanted with TGF-β3 expressing cells in which collagen bundles were uniformly parallel and organized.

DISCUSSION

This study shows that continuous delivery of TGF-β3 during the initial days of wound healing by an engineered marrow stromal cell improves the cosmetic appearance of the scar without negatively affecting the process of tissue repair. Local delivery of recombinant, active TGF-β3 to the wound margins was approved for a phase III clinical trial. However, the trial has been discontinued as it was not as effective as it was expected (16). This could be attributed to the low half-life of the active TGF-β3, which is only 2–3 min in plasma (34). On the other hand, it has been shown in a mouse model that if the level of active TGF-β3 is highly increased following a lentiviral gene delivery to the site of skin wound, it decreases the wound re-epithelialization in addition to reduction of scar tissue formation (5). We hypothesized that temporary

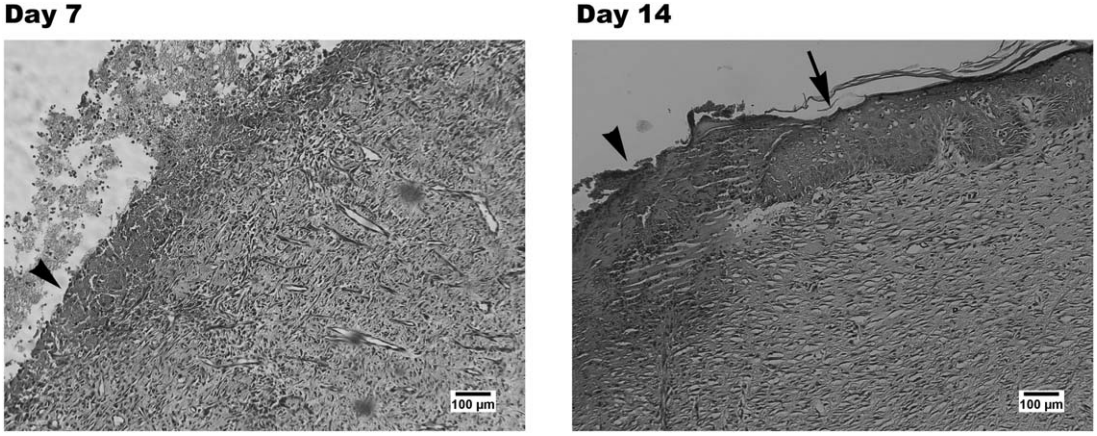

FIG. 7. H&E staining of epithelialized wound area. The wounded skin started to epithelialize from the margins in all groups. On day 7, a fragile epithelium was identified which progressed to a multi-layer and more stable epithelium from day 14 onwards. Arrow heads show the newly formed and the arrow indicates the untouched epithelia (40× magnification; control group with no implantation).

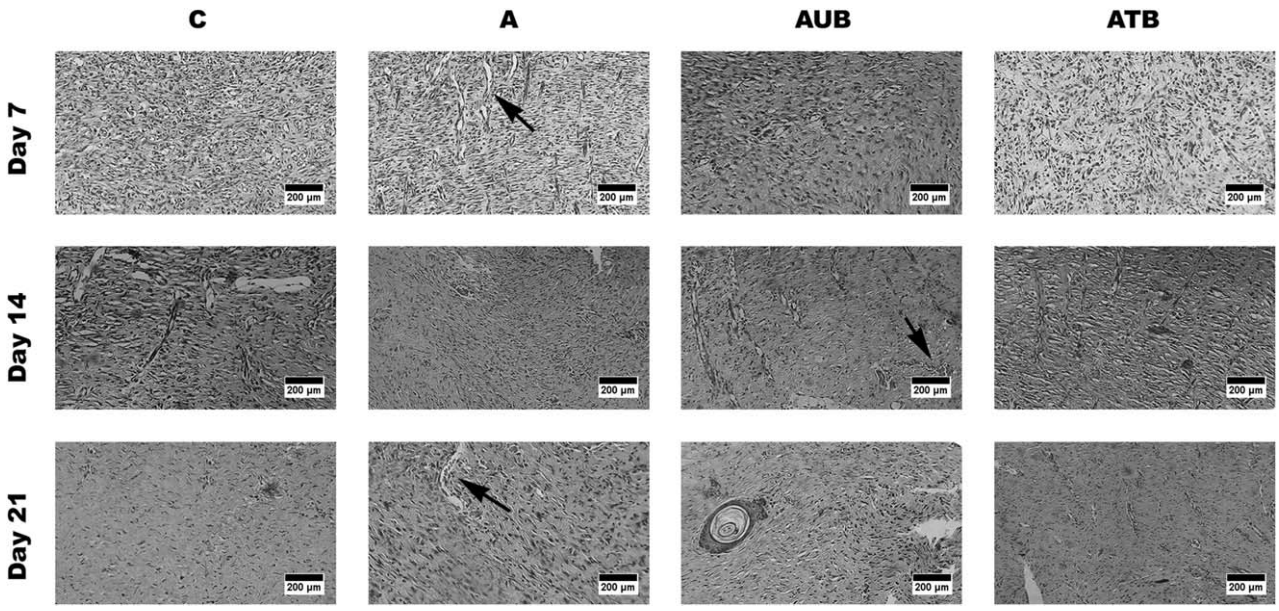

FIG. 8. H&E staining of the healing dermis. The granulation tissue was observed on the first postoperative sampling on day 7 and matured in subsequent days. From days 7 through 21, the cellularity and vascularity of the healing dermis decreased, but the pattern was fairly the same in all experimental groups. Arrows show the vascular structures; (10× magnification). C, control group with no implantation; A, group implanted with human dehydrated amniotic membrane (hDAM) alone; AUB, group implanted with the hDAM seeded with untransfected bone marrow stromal cells (BM-SCs); ATB, group implanted with the hDAM seeded with the transfected BM-SCs.

and continuous delivery of TGF-β3 by marrow stromal cells on amniotic membrane can modulate the negative effect of high level of TGF-β3 on wound healing while keeping the scar reduction effects of this growth factor.

We constructed a recombinant plasmid pcDNA3.1-TGF-β3 expression system by isolation of TGF-β3 cDNA from pGEM-T-TGF-β3 cloning vector and its subcloning into pcDNA3.1 plasmid vector. The accuracy of construction was confirmed by electrophoretic movement of the construct, and the PCR amplification and sequencing of the subcloned TGF-β3. Then, we transfected the bone marrow stromal cells seeded on amniotic membrane and confirmed the success of transfection by RT-PCR of TGF-β3 mRNA and Western blotting. As expression of TGF-β3 mRNA and protein were detectable from day 3 through 7 after transfection, the transfected marrow stromal cells-amniotic membrane constructs were implanted at day three post-transfection.

Our in vivo experiment demonstrated that this construct does not negatively affect the rate of wound contraction, epithelialization, and formation of granulation tissue. Counting of the cells in the healing dermis on day 7 showed a high number of cells in AUB group, which is due to delivery of stromal cells to the wound in this group. In the wounds implanted with the transfected cells, the number of the cells on day 7 were lower than other groups, even the controls. This shows that TGF-β3 decreases the retention of the cells in the wound area during the early phase of healing. The decrease of cell numbers in the AUB group on day 14 and very slight increase in ATB indicated that in

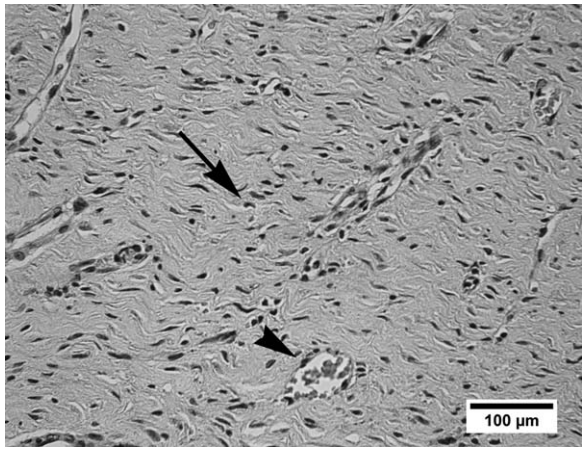

FIG. 9. H&E-stained field for counting cell nuclei and vascular structures. The representative photomicrograph of the field used for counting cell nuclei (arrow) and vascular structures (arrowhead) (40× magnification; day 21 of the sample implanted with the hDAM seeded with the transfected BM-SCs). In each slide, the nuclei and vascular structures were counted in three fields and averaged for statistical analysis.

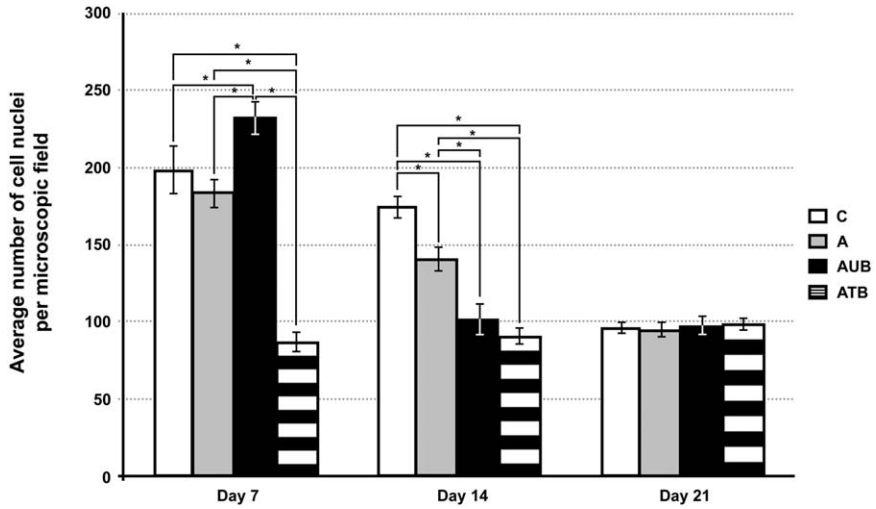

FIG. 10. The mean cell nuclei counts in healing dermis. Total number of cells were counted by enumeration of nuclei in day 7, 14, and 21 samples and presented by mean ± SEM. Statistically significant differences are marked by an asterisk. C, control group with no implantation; A, group implanted with human dehydrated amniotic membrane (hDAM) alone; AUB, group implanted with the hDAM seeded with untransfected bone marrow stromal cells (BM-SCs); ATB, group implanted with the hDAM seeded with the transfected BM-SCs.

this microenvironment, bone marrow stromal cells decrease recruitment of cells (including inflammatory cells) to the healing area but TGF-β3 retain the engrafted cells in the area. Lack of significant difference in cell counting between the experimental groups on day 21 shows that our engineered dermal equivalent may not affect the dynamics of cell movements during the late stage of wound healing. Although we do not report the type of the cells, including inflammatory cells, further studies to determine the types of the inflammatory cells and their dynamics in the wound after application of this dermal equivalent will provide valuable data.

Count of vascular structures showed that amniotic membrane alone (day 21) and that seeded with untransfected stromal cells (days 14 and 21) and transfected cells (day 21) (Fig. 11) decrease the formation of vascular structures in the healing dermis as compared to controls. Our findings are in line with previous studies, which reported that

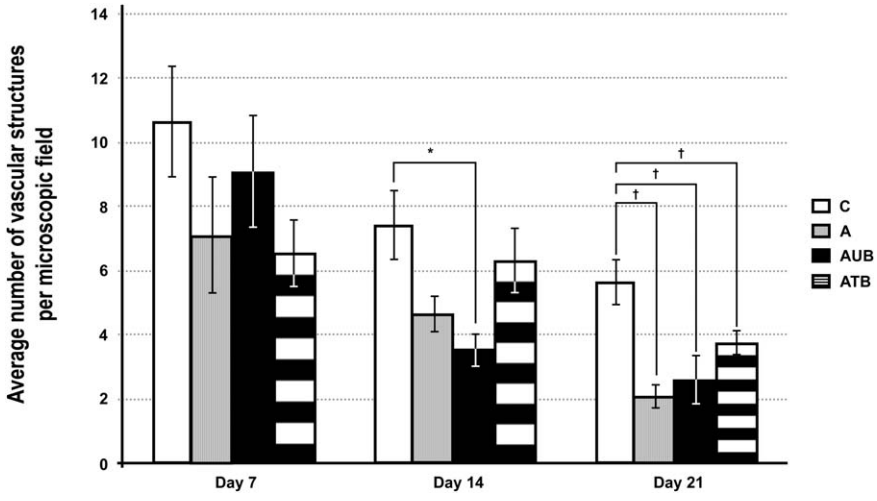

FIG. 11. The mean vascular structure counts in the healing dermis. The number of vascular structures were counted in days 7 through 21 and presented by mean ± SEM. Statistically significant differences are marked. *Significant difference shown by Kruskal–Wallis one-way ANOVA with "all pair-wise" comparisons; †significant difference shown by one-way ANOVA followed by Tukey's post hoc test; C, control group with no implantation; A, group implanted with human dehydrated amniotic membrane (hDAM) alone; AUB, group implanted with the hDAM seeded with untransfected bone marrow stromal cells (BM-SCs); ATB, group implanted with the hDAM seeded with the transfected BM-SCs.

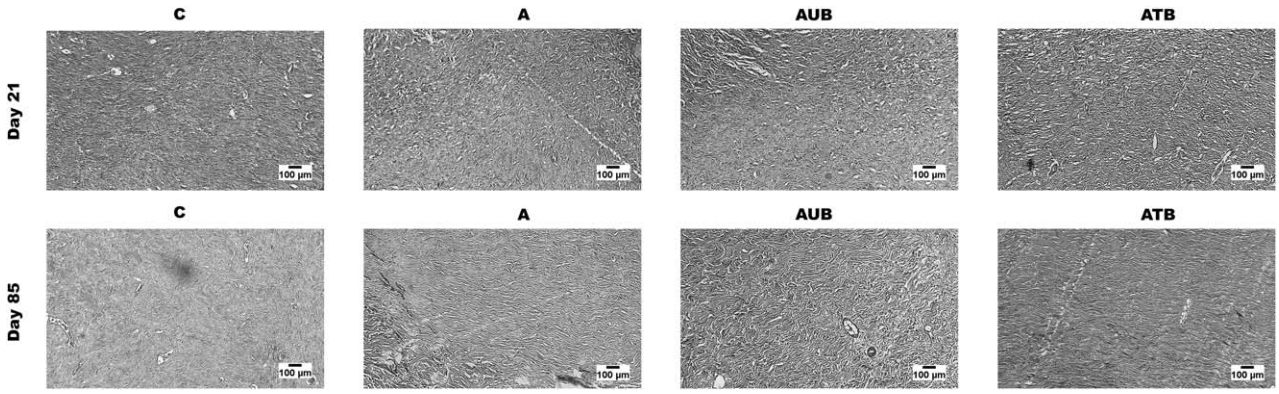

FIG. 12. Masson's trichrome staining of the healing dermis. The staining shows the orientation of the collagen fibers on days 21 and 85 after operation. The most organized and parallel collagen bundles are observed in ATB experimental group on day 85; (10× magnification). C, control group with no implantation; A, group implanted with human dehydrated amniotic membrane (hDAM) alone; AUB, group implanted with the hDAM seeded with untransfected bone marrow stromal cells (BM-SCs); ATB, group implanted with the hDAM seeded with the transfected BM-SCs.

reduction of wound vascularity is associated with decreased scar formation (35) and that higher level of angiogenesis is observed in hypertrophic scars (36). As a result, it has been suggested that anti-angiogenesis would be a possible modality for scarless wound healing (37). However, it should be noted that a minimum level of angiogenesis is essential for wound healing. There are several studies that have linked inadequate angiogenesis with poor wound healing, especially in chronic conditions such as diabetes (38,39) and venous stasis (40). Although our dermal equivalent has decreased angiogenesis in the wound, the decrease was not to the level that negatively affected the process of healing and instead, contributed to reduction of scar formation.

The other effect of our engineered dermal implant was the formation of uniformly parallel and organized collagen bundles, which led to a high improvement of the cosmetic appearance of the scar. The relationship between organization of collagen bundles and appearance of the scar has been described in earlier reports (see Wolfram et al. [41], Armour et al. [42], and Xue et al. [43]). These results conform to the earlier reports that show the ratio of TGF-β1 and 2 to TGF-β3 is an important determinant of scar formation. For example, by administration of TGF-β1 and 2 neutralizing antibodies and exogenous TGF-β3 during the first 48 hours after wounding, Shah et al. (11) demonstrated that decreasing the ratio of TGF-β1,2/TGF-β3 reduces the ECM deposition, improves the architecture of neodermis and reduces the scar formation . Interestingly, a report published by Wu et al. (12) shows that if the ratio of TGF-β1,2/TGF-β3 is not decreased to a certain point, the process of scar formation will not be affected.

The safety of plasmid gene delivery method used in the current study is higher than the viral methods in terms of immunogenicity and insertional mutagenesis (see Wang et al., 2014 for review [44]). The transient nature of transfection and increased expression of TGF-β3 only during days 3–7 post-transfection provides an additional index of safety. In recent years, several studies have been performed to examine the effects of growth factors on microenvironmental modulation (45–48) and the role of marrow stromal cells in wound healing. It has been shown that these can attenuate the inflammatory response in the wound by suppressing the proliferation of natural killer cells (49) and T cells (50), and modulating the response of immune cells to increase the secretion of anti-inflammatory cytokines such as IL-10 and IL-35 and decrease the secretion of pro-inflammatory cytokines such as TNF-α and interferon-γ (51). Additionally, these cells secrete factors like vascular endothelial growth factor, which stimulates angiogenesis and promotes the development of granulation tissue (52). These cells promote wound re-epithelialization by a cross-talk with keratinocytes and activation of a number of signaling pathways including KGF signaling (53). Secretion of anti-fibrotic factors like IL-10 and hepatocyte growth factor (54) is another mechanism of contribution of these cells to the wound healing. Although, in the present study, the mechanism of regulation of wound healing may be significantly different from the studies aforementioned, it could be speculated that the marrow stromal cells have modulated the effects of TGF-β3 on the

wound healing and re-epithelialization and contributed to the timely closure of the wound while keeping the fibrosis at the minimum possible level.

CONCLUSION

In summary, the results of the current study showed that a surgically created experimental skin wound heals with minimal scarring if implanted with a construct made up of human dehydrated amniotic membrane and genetically modified marrow stromal cells, which temporary secrete transforming growth factor beta-3 protein during the early phase of wound healing.

Acknowledgments: This study was funded by grants from the Iran National Science Foundation (INSF) and Iran University of Medical Sciences. The authors would like to thank Ms. Mahshid Mohammadipour (the Research Center, Iranian Blood Transfusion Organization, Tehran, Iran) for her technical assistance.

Authors' contributions: Conceived the project: Samadikuchaksaraei. Designed the experiments: Samadikuchaksaraei, Verdi, Joghataei, As'adi and Habibi Roudkenar. Performed the experiments: Mehdipour, Amiri, Dehghan Harati, and Gholipourmalekabadi. Analyzed the data: Samadikuchaksaraei and Karkuki Osguei. Contributed reagents/materials/analysis tools: Samadikuchaksaraei, Habibi Roudkenar and As'adi. Wrote the paper: Samadikuchaksaraei. Prepared the illustrations: Samadikuchaksaraei. Interpreted the results: Samadikuchaksaraei and Mehdipour. Corrected the manuscript and approved its final version: Samadikuchaksaraei, Mehdipour, Verdi, Joghataei, As'adi, Amiri, Dehghan Harati, Gholipourmalekabadi, Karkuki Osguei.

Conflict of Interest: Authors have no conflict of interest.

REFERENCES

1. Tziotzios C, Profyris C, Sterling J. Cutaneous scarring: pathophysiology, molecular mechanisms, and scar reduction therapeutics Part II. Strategies to reduce scar formation after dermatologic procedures. *J Am Acad Dermatol* 2012; 66:13–24.
2. Lu L, Saulis AS, Liu WR, et al. The temporal effects of anti-TGF-beta1, 2, and 3 monoclonal antibody on wound healing and hypertrophic scar formation. *J Am Coll Surg* 2005;201:391–7.
3. Finnson KW, Arany PR, Philip A. Transforming growth factor beta signaling in cutaneous wound healing: lessons learned from animal studies. *Adv Wound Care* 2013;2: 225–37.
4. Pakyari M, Farrokhi A, Maharlooei MK, Ghahary A. Critical role of transforming growth factor beta in different phases of wound healing. *Adv Wound Care* 2013;2:215–24.
5. Waddington SN, Crossley R, Sheard V, et al. Gene delivery of a mutant TGFbeta3 reduces markers of scar tissue formation after cutaneous wounding. *Mol Ther* 2010;18: 2104–11.
6. Zheng Z, Nguyen C, Zhang X, et al. Delayed wound closure in fibromodulin-deficient mice is associated with increased TGF-beta3 signaling. *J Invest Dermatol* 2011;131: 769–78.
7. Schrementi ME, Ferreira AM, Zender C, DiPietro LA. Site-specific production of TGF-beta in oral mucosal and cutaneous wounds. *Wound Repair Regen* 2008;16:80–6.
8. Occleston NL, O'Kane S, Laverty HG, et al. Discovery and development of avotermin (recombinant human transforming growth factor beta 3): a new class of prophylactic therapeutic for the improvement of scarring. *Wound Repair Regen* 2011;19(Suppl. 1):s38–48.
9. Ferguson MW, O'Kane S. Scar-free healing: from embryonic mechanisms to adult therapeutic intervention. *Philos Trans R Soc Lond Ser B Biol Sci* 2004;359:839–50.
10. Bandyopadhyay B, Fan J, Guan S, et al. A "traffic control" role for TGFbeta3: orchestrating dermal and epidermal cell motility during wound healing. *J Cell Biol* 2006; 172:1093–105.
11. Shah M, Foreman DM, Ferguson MW. Neutralisation of TGF-beta 1 and TGF-beta 2 or exogenous addition of TGF-beta 3 to cutaneous rat wounds reduces scarring. *J Cell Sci* 1995;108:985–1002.
12. Wu L, Siddiqui A, Morris DE, Cox DA, Roth SI, Mustoe TA. Transforming growth factor beta 3 (TGF beta 3) accelerates wound healing without alteration of scar prominence. Histologic and competitive reverse-transcription-polymerase chain reaction studies. *Arch Surg* 1997;132:753–60.
13. Hosokawa R, Nonaka K, Morifuji M, Shum L, Ohishi M. TGF-beta 3 decreases type I collagen and scarring after labioplasty. *J Dent Res* 2003;82:558–64.
14. Laverty HG, Occleston NL, Johnson M, et al. Effects of avotermin (transforming growth factor beta3) in a clinically relevant pig model of long, full-thickness incisional wounds. *J Cutan Med Surg* 2010;14:223–32.
15. Ferguson MW, Duncan J, Bond J, et al. Prophylactic administration of avotermin for improvement of skin scarring: three double-blind, placebo-controlled, phase I/II studies. *Lancet* 2009;373:1264–74.
16. Gauglitz GG. Management of keloids and hypertrophic scars: current and emerging options. *Clin Cosmet Investig Dermatol* 2013;6:103–14.
17. Saki M, Narbat MK, Samadikuchaksaraei A, Ghafouri HB, Gorjipour F. Biocompatibility study of a hydroxyapatite-alumina and silicon carbide composite scaffold for bone tissue engineering. *Yakhteh* 2009;11:55–60.
18. Mobini S, Hoyer B, Solati-Hashjin M, et al. Fabrication and characterization of regenerated silk scaffolds reinforced with natural silk fibers for bone tissue engineering. *J Biomed Mater Res Part A* 2013;101:2392–404.
19. Mobini S, Solati-Hashjin M, Peirovi H, et al. Bioactivity and biocompatibility studies on silk-based scaffold for bone tissue engineering. *J Med Biol Eng* 2013;33:207–14.
20. Jafari J, Emami SH, Samadikuchaksaraei A, Bahar MA, Gorjipour F. Electrospun chitosan-gelatin nanofiberous scaffold: fabrication and in vitro evaluation. *Biomed Mater Eng* 2011;21:99–112.
21. Gholipourmalekabadi M, Mozafari M, Salehi M, et al. Development of a cost-effective and simple protocol for decellularization and preservation of human amniotic membrane as a soft tissue replacement and delivery system for bone marrow stromal cells. *Adv Healthc Mater* 2015;4:918–26.
22. Koob TJ, Lim JJ, Zabek N, Massee M. Cytokines in single layer amnion allografts compared to multilayer amnion/

chorion allografts for wound healing. *J Biomed Mater Res Part B Appl Biomater* 2015;103:1133–40.
23. Seeger MA, Paller AS. The roles of growth factors in keratinocyte migration. *Adv Wound Care* 2015;4:213–24.
24. Schultz GS, Davidson JM, Kirsner RS, Bornstein P, Herman IM. Dynamic reciprocity in the wound microenvironment. *Wound Repair Regen* 2011;19:134–48.
25. Koob TJ, Lim JJ, Massee M, Zabek N, Denoziere G. Properties of dehydrated human amnion/chorion composite grafts: implications for wound repair and soft tissue regeneration. *J Biomed Mater Res Part B Appl Biomater* 2014; 102:1353–62.
26. Rocha SCM, Baptista CJM. Biochemical properties of amniotic membrane. In: Mamede AC, Botelho MF, eds. *Amniotic Membrane*. The Netherlands: Springer, 2015;19–40.
27. Kang M, Choi S, Cho Lee AR. Effect of freeze dried bovine amniotic membrane extract on full thickness wound healing. *Arch Pharm Res* 2013;36:472–8.
28. Cheng J, Yu H, Deng S, Shen G. MicroRNA profiling in mid- and late-gestational fetal skin: implication for scarless wound healing. *Tohoku J Exp Med* 2010;221:203–9.
29. Shenoy RR, Sudheendra AT, Nayak PG, Paul P, Kutty NG, Rao CM. Normal and delayed wound healing is improved by sesamol, an active constituent of *Sesamum indicum* (L.) in albino rats. *J Ethnopharmacol* 2011;133: 608–12.
30. Beausang E, Floyd H, Dunn KW, Orton CI, Ferguson MW. A new quantitative scale for clinical scar assessment. *Plast Reconstr Surg* 1998;102:1954–61.
31. Fearmonti R, Bond J, Erdmann D, Levinson H. A review of scar scales and scar measuring devices. *Eplasty* 2010;10:e43.
32. Tomlinson A, Ferguson MW. Wound healing: a model of dermal wound repair. *Methods Mol Biol* 2003;225:249–60.
33. Zwingenberger S, Langanke R, Vater C, et al. The effect of SDF-1alpha on low dose BMP-2 mediated bone regeneration by release from heparinized mineralized collagen type I matrix scaffolds in a murine critical size bone defect model. *J Biomed Mater Res Part A* 2016;104:2126–34.
34. Wakefield LM, Winokur TS, Hollands RS, Christopherson K, Levinson AD, Sporn MB. Recombinant latent transforming growth factor beta 1 has a longer plasma half-life in rats than active transforming growth factor beta 1, and a different tissue distribution. *J Clin Invest* 1990;86:1976–84.
35. Wilgus TA, Ferreira AM, Oberyszyn TM, Bergdall VK, Dipietro LA. Regulation of scar formation by vascular endothelial growth factor. *Lab Invest* 2008;88:579–90.
36. van der Veer WM, Niessen FB, Ferreira JA, et al. Time course of the angiogenic response during normotrophic and hypertrophic scar formation in humans. *Wound Repair Regen* 2011;19:292–301.
37. Diao JS, Xia WS, Guo SZ. Bevacizumab: a potential agent for prevention and treatment of hypertrophic scar. *Burns* 2010;36:1136.
38. Lim YC, Bhatt MP, Kwon MH, et al. Proinsulin C-peptide prevents impaired wound healing by activating angiogenesis in diabetes. *J Invest Dermatol* 2015;135:269–78.
39. Bizenjima T, Seshima F, Ishizuka Y, Takeuchi T, Kinumatsu T, Saito A. Fibroblast growth factor-2 promotes healing of surgically created periodontal defects in rats with early, streptozotocin-induced diabetes via increasing cell proliferation and regulating angiogenesis. *J Clin Periodontol* 2015;42:62–71.
40. Drinkwater SL, Burnand KG, Ding R, Smith A. Increased but ineffectual angiogenic drive in nonhealing venous leg ulcers. *J Vasc Surg* 2003;38:1106–12.
41. Wolfram D, Tzankov A, Pulzl P, Piza-Katzer H. Hypertrophic scars and keloids—a review of their pathophysiology, risk factors, and therapeutic management. *Dermatol Surg* 2009;35:171–81.
42. Armour A, Scott PG, Tredget EE. Cellular and molecular pathology of HTS: basis for treatment. *Wound Repair Regen* 2007;15 (Suppl. 1):S6–17.
43. Xue M, Jackson CJ. Extracellular matrix reorganization during wound healing and its impact on abnormal scarring. *Adv Wound Care* 2015;4:119–36.
44. Wang W, Xu X, Li Z, Lendlein A, Ma N. Genetic engineering of mesenchymal stem cells by non-viral gene delivery. *Clin Hemorheol Microcirc* 2014;58:19–48.
45. Samadikuchaksaraei A, Bishop AE. Effects of growth factors on the differentiation of murine ESC into type II pneumocytes. *Cloning Stem Cells* 2007;9:407–16.
46. Van Vranken BE, Rippon HJ, Samadikuchaksaraei A, Trounson AO, Bishop AE. The differentiation of distal lung epithelium from embryonic stem cells. *Curr Protoc Stem Cell Biol* 2007; Chapter 1:Unit 1G.
47. Samadikuchaksaraei A, Bishop AE. Derivation and characterization of alveolar epithelial cells from murine embryonic stem cells in vitro. *Methods Mol Biol* 2006;330:233–48.
48. Siti-Ismail N, Samadikuchaksaraei A, Bishop AE, Polak JM, Mantalaris A. Development of a novel three-dimensional, automatable and integrated bioprocess for the differentiation of embryonic stem cells into pulmonary alveolar cells in a rotating vessel bioreactor system. *Tissue Eng Part C Methods* 2012;18:263–72.
49. Spaggiari GM, Capobianco A, Abdelrazik H, Becchetti F, Mingari MC, Moretta L. Mesenchymal stem cells inhibit natural killer-cell proliferation, cytotoxicity, and cytokine production: role of indoleamine 2,3-dioxygenase and prostaglandin E2. *Blood* 2008;111:1327–33.
50. Yang SH, Park MJ, Yoon IH, et al. Soluble mediators from mesenchymal stem cells suppress T cell proliferation by inducing IL-10. *Exp Mol Med* 2009;41:315–24.
51. Aggarwal S, Pittenger MF. Human mesenchymal stem cells modulate allogeneic immune cell responses. *Blood* 2005; 105:1815–22.
52. Wang Y, Crisostomo PR, Wang M, Markel TA, Novotny NM, Meldrum DR. TGF-alpha increases human mesenchymal stem cell-secreted VEGF by MEK- and PI3-K- but not JNK- or ERK-dependent mechanisms. *Am J Physiol Regul Integr Comp Physiol* 2008;295:R1115–23.
53. Menon SN, Flegg JA, McCue SW, Schugart RC, Dawson RA, McElwain DL. Modelling the interaction of keratinocytes and fibroblasts during normal and abnormal wound healing processes. *Proc Biol Sci* 2012;279:3329–38.
54. Jackson WM, Nesti LJ, Tuan RS. Mesenchymal stem cell therapy for attenuation of scar formation during wound healing. *Stem Cell Res Ther* 2012;3:20.